Acidification-driven fractional viscoelasticity of yoghurt gelation: a pH-parameterised springpot model from the gel point to the set gel

Abdelmajid Benahmed
Conservatoire National des Arts et Métiers (CNAM), France
abenahmed1@gmail.com

November 2026

Abstract

In yoghurt plants, incubation is stopped when the pH reaches a target value, yet the texture of the product is decided earlier, while the casein network is being built. This paper asks whether the dynamic moduli $G'(\omega, t)$ and $G''(\omega, t)$ of a fermenting milk can be predicted from its pH curve once the gel point has been passed. The model has three stages. A modified Gompertz law (or any mechanistic fermentation model) gives the pH; gelation is placed at the pH pH_g where the Winter–Chambon criterion holds; beyond that point the gel is a springpot whose exponent and modulus are functions of pH. We study two versions, one in which the exponent follows pH instantly (Option A) and one in which it relaxes towards its equilibrium value through a Caputo equation (Option B). Writing the quasi-property as $\mathbb{V} = G_0\,\omega_0^{-\alpha}$ removes the dependence on the time unit, and placing ω_0 at the logarithmic centre of the measured band lowers the correlation between $\ln G_0$ and α. With Pollard's theorem we show that, in Option B, α cannot leave the interval between its terminal and critical values. Creep simulations bring out a less expected point: if the prefactor of a variable-order law is kept outside the hereditary integral, the computed strain decreases under constant stress once the mutation number approaches one. Moving $\mathbb{V}(s)$ inside the integral, so that new bonds form without stress, removes this artefact. For a slow starter culture, 5 s chirps keep the mutation number below 0.03, and the quasi-static approximation is then within 2% of the full creep solution. On synthetic data, one fermentation is not enough to identify the lag parameters of Option B, but three acidification rates fitted together are. The paper contains no new laboratory data; we describe the experiments that would test the model.

Keywords: fractional viscoelasticity; acid milk gelation; yoghurt; springpot; variable-order operators; mutation number; structural identifiability.

1 Introduction

In yoghurt manufacture the firmness of the gel is fixed during incubation, but what operators follow in real time is the pH. The two sides of the process are also modelled separately. Fermentation models describe how acid develops, without saying anything about frequency-dependent moduli [16]. Fractional rheological models, for their part, describe mature dairy gels with very few parameters but ignore the acidification history that produced those gels [1, 2].

Several pieces of a coupled model can already be found in the literature. Scott Blair's springpot has been used for semi-hard cheeses [1] and for caseinate gels acidified with glucono-δ-lactone (GDL); in the latter case a two-parameter fit gives $\alpha = 0.18 \pm 0.01$ for a gel at 4% casein [4]. Wagner et al. applied fractional Maxwell and Jeffreys models to liquid foods [2]. The closest work to ours is a conference abstract by Divoux, Keshavarz and Leocmach on caseinate–GDL mixtures, in which

power-law rheology appears at the gel point and the exponent then falls towards a terminal value [5]. As far as we can tell from the abstract, no law $\alpha(\mathrm{pH})$ is proposed and starter-fermented milk is not considered. For rennet gels, Bauland et al. used a fractional Poynting–Thomson model; at a casein volume fraction of 10% they report a gel time of 1770 s, a critical exponent of 0.62, and time–connectivity superposition [9]. Joshi has recently written physically constrained fractional models on both sides of the gel point with Mittag–Leffler–Prabhakar functions, with no dairy application [10]. Measurement is not the bottleneck any more: optimally windowed chirps (OWCh) record a full spectrum in a few seconds [6, 8], much less than the mutation time of about 120 s expected for the GDL–caseinate gel studied by Geri et al. [6]. One caution applies to all GDL results, however. Özcan, Horne and Lucey point out that GDL gels can differ markedly, in texture and physical properties, from gels set by starter cultures [15], and what is learned on the former cannot be carried over to yoghurt without checking.

We have not found a study that brings together (i) a springpot whose parameters are explicit functions of pH and which starts from the Winter–Chambon critical gel, (ii) a quantitative comparison, based on the mutation number, of the quasi-static approximation with genuine variable-order laws, and (iii) a link to starter-driven acidification whose end state can be passed on to a model of a stirred-yoghurt line.

The question we address is the following: under which mathematical and metrological conditions can $G'(\omega, t)$ and $G''(\omega, t)$ of a starter-fermented milk be predicted from its pH trajectory alone, with a fractional law of few parameters? We do not yet have access to multi-frequency rheometry coupled to pH measurements on fermenting milk, and the paper is restricted to theory and simulation. We write down the constitutive equations, prove two properties of the model, test the numerical schemes and the identifiability of the parameters on synthetic data, and describe the laboratory campaign that the model now needs.

2 Physical and mathematical background

2.1 Acid gelation of milk and thermal pretreatment

As the pH falls, the κ-casein layer that keeps casein micelles apart loses much of its negative charge, and colloidal calcium phosphate is progressively dissolved. In unheated milk the sol–gel transition takes place near $\mathrm{pH}_g \approx 4.9$ [14]. Yoghurt milk is usually heated before inoculation (Soukoulis et al. used, for example, 80°C for 30 min [16]). Heating denatures the whey proteins, mainly β-lactoglobulin, whose isoelectric point is close to 5.3; once associated with the micelles, they shift gelation to a higher pH [14]. Temperature matters as well. In pre-heated milk fermented by lactic bacteria, Laligant et al. measured a gel pH of 5.24 ± 0.13 at 30°C and of 5.53 ± 0.01 at 42°C, although G' at pH 4.6 came out the same at both temperatures [18]. Fermentation times vary too: in a study covering 36 to 44°C and 1 to 3% inoculum, the first two phases lasted between 4.5 and 7 h [17]. Laligant et al. also discuss a limited transfer of acid and protons from the serum to the colloidal phase, which makes the gel heterogeneous [18]. A pH probe may thus read a value that the network has not yet reached.

2.2 Constant-order fractional operators and critical gelation

Let $t_0 \in \mathbb{R}$, $T > t_0$, and let $\gamma \in AC([t_0, T])$ denote an absolutely continuous shear-strain history with integrable strain rate $\dot{\gamma} \in L^1(t_0, T)$. For a constant fractional order $\alpha \in (0, 1)$, the left-sided Caputo derivative is defined for almost every $t \in (t_0, T]$ by

$$ {}^{C}D^{\alpha}_{t_0}\gamma(t) = \frac{1}{\Gamma(1-\alpha)} \int_{t_0}^{t} (t-s)^{-\alpha}\, \dot{\gamma}(s)\, ds, \tag{1} $$

where $\Gamma(\cdot)$ is the Euler gamma function. Scott Blair's springpot relates shear stress $\sigma(t)$ (Pa) to dimensionless shear strain $\gamma(t)$ through

$$\sigma(t) = \mathbb{V}\, {}^{C}D^{\alpha}_{t_0}\gamma(t), \qquad \mathbb{V} > 0, \quad \alpha \in (0,1), \tag{2}$$

where the quasi-property $\mathbb{V}$ carries fractional units $[\mathbb{V}] = \mathrm{Pa\,s}^{\alpha}$. Taking $\alpha \to 0^{+}$ recovers a Hookean elastic solid (assuming $\gamma(t_0) = 0$), while $\alpha \to 1^{-}$ recovers a Newtonian fluid.

Under steady small-amplitude oscillatory shear ($\gamma(t) = \gamma_0 e^{i\omega t}$, $t_0 \to -\infty$, $\omega > 0$), the Fourier transform of (1) yields the complex modulus $G^{*}(\omega) = \mathbb{V}(i\omega)^{\alpha} = G'(\omega) + iG''(\omega)$ [3]:

$$G'(\omega) = \mathbb{V}\,\omega^{\alpha}\cos\!\left(\frac{\pi\alpha}{2}\right), \qquad G''(\omega) = \mathbb{V}\,\omega^{\alpha}\sin\!\left(\frac{\pi\alpha}{2}\right), \qquad \tan\delta(\omega) = \frac{G''(\omega)}{G'(\omega)} = \tan\!\left(\frac{\pi\alpha}{2}\right). \tag{3}$$

By the Winter–Chambon criterion [21], the gel point t_g is reached when $\tan\delta(\omega, t_g)$ becomes frequency-independent, corresponding to congruent power-law moduli $G'(\omega, t_g) \propto G''(\omega, t_g) \propto \omega^{n}$ with critical exponent $n \in (0,1)$.

2.3 Variable-order operators and breakdown of Boltzmann superposition

Once α changes with time, say along $\alpha : [t_g, T] \to (0,1)$, there is more than one way to generalise (1). Three definitions are common in mechanics:

1. *Type-I Caputo derivative* (order evaluated at the current time t):

$$ {}^{C}D^{\alpha(t),\mathrm{I}}_{t_0}\gamma(t) = \frac{1}{\Gamma(1-\alpha(t))}\int_{t_0}^{t}(t-s)^{-\alpha(t)}\,\dot\gamma(s)\,ds.$$

2. *Type-II Caputo derivative* (order evaluated at the past integration time s):

$$ {}^{C}D^{\alpha(\cdot),\mathrm{II}}_{t_0}\gamma(t) = \int_{t_0}^{t}\frac{(t-s)^{-\alpha(s)}}{\Gamma(1-\alpha(s))}\,\dot\gamma(s)\,ds.$$

3. *Scarpi derivative* [12, 11], defined through the Laplace domain. Giusti et al. point out that, to their knowledge, it is the only variable-order framework consistent with the theory of general fractional operators [11].

None of them has a kernel of the form $K(t-s)$, and the Boltzmann superposition principle is lost [13]. This has a practical consequence: an oscillatory measurement can be read through a stationary Fourier transform only if the material hardly changes while it is being measured.

3 Coupled constitutive formulation

The four stages of the model, from processing conditions to linear viscoelastic spectra and on to a stirred-yoghurt line model, are sketched in Figure 1.

3.1 Acidification kinetics and closed-form gel time

Following Soukoulis et al. [16], empirical pH decline for $t \geq 0$ is described by the modified Gompertz equation:

$$\mathrm{pH}(t) = \mathrm{pH}_0 - A\,\exp\!\left\{-\exp\!\left[\frac{\mu_m e}{A}(\lambda - t) + 1\right]\right\}, \tag{4}$$

where $\mathrm{pH}_0 > 0$ is the asymptotic initial pH, $A > 0$ is the total pH drop ($\mathrm{pH}_\infty = \mathrm{pH}_0 - A$), $\mu_m > 0$ is the maximum acidification rate, $\lambda \geq 0$ is the lag time, and $e = \exp(1)$.

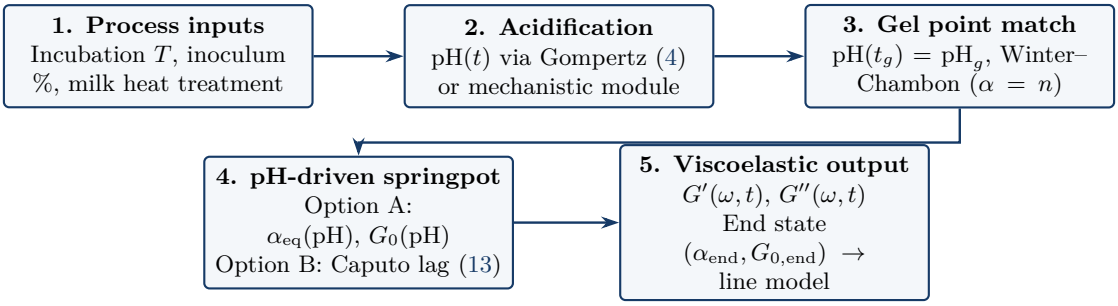

Figure 1: Structure of the model: fermentation conditions, acidification, gel point and pH-driven springpot, with the end-of-incubation state passed to a stirred-yoghurt line simulator.

Proposition 1 (Uniqueness of t_g and boundary offset at $t = 0$)**.** *Let $A > 0$ and $\mu_m > 0$.*

1. *The map $t \mapsto \mathrm{pH}(t)$ in (4) belongs to $C^\infty(\mathbb{R})$, is strictly decreasing on $\mathbb{R}$, and attains its steepest slope $-\mu_m$ at the unique inflection time $t_{\mathrm{infl}} = \lambda + A/(\mu_m e)$.*

2. *For every gelation threshold $\mathrm{pH}_g \in (\mathrm{pH}_0 - A,\, \mathrm{pH}(0))$, the equation $\mathrm{pH}(t_g) = \mathrm{pH}_g$ admits a unique positive solution:*

$$t_g = \lambda + \frac{A}{\mu_m e}\left\{1 - \ln\left[-\ln\left(\frac{\mathrm{pH}_0 - \mathrm{pH}_g}{A}\right)\right]\right\}. \tag{5}$$

3. *At $t = 0$, (4) exhibits a strictly positive residual offset $\delta_0 = \mathrm{pH}_0 - \mathrm{pH}(0) = A\exp\big(-\exp(\frac{\mu_m e}{A}\lambda + 1)\big) > 0$.*

Proof. Set $u(t) = \frac{\mu_m e}{A}(\lambda - t) + 1$, so $u'(t) = -\frac{\mu_m e}{A}$. Applying the chain rule to (4) gives

$$\dot{\mathrm{pH}}(t) = -\mu_m e \exp\big(u(t) - e^{u(t)}\big) < 0 \qquad \forall t \in \mathbb{R},$$

establishing strict monotonicity and bijectivity onto $(\mathrm{pH}_0 - A, \mathrm{pH}_0)$. Differentiating once more gives $\ddot{\mathrm{pH}}(t) = \frac{(\mu_m e)^2}{A}(1 - e^{u(t)})\exp(u(t) - e^{u(t)})$, which vanishes solely at $u = 0$, i.e., $t_{\mathrm{infl}} = \lambda + A/(\mu_m e)$, where $\dot{\mathrm{pH}}(t_{\mathrm{infl}}) = -\mu_m e \cdot e^{-1} = -\mu_m$. For $\mathrm{pH}_g \in (\mathrm{pH}_0 - A, \mathrm{pH}(0))$, the ratio $(\mathrm{pH}_0 - \mathrm{pH}_g)/A$ lies in $(0, 1)$, so its logarithm is strictly negative; inverting $\exp(-e^{u(t_g)}) = (\mathrm{pH}_0 - \mathrm{pH}_g)/A$ yields (5), and $\mathrm{pH}_g < \mathrm{pH}(0)$ ensures $t_g > 0$. Evaluating (4) at $t = 0$ gives δ_0 directly. □

Take a heated milk with $\mathrm{pH}_0 = 6.65$, $A = 2.15$, $\mu_m = 0.70\,\mathrm{pH\,h^{-1}}$ and $\lambda = 1.50\,\mathrm{h}$. The offset is then $\delta_0 = 7.6 \times 10^{-5}$ pH units, well below what a probe can resolve (± 0.01). The curve has its inflection at $t_{\mathrm{infl}} = 2.63\,\mathrm{h}$; the gel forms at $t_g = 3.68\,\mathrm{h}$ if $\mathrm{pH}_g = 5.20$, or at $4.42\,\mathrm{h}$ if $\mathrm{pH}_g = 4.90$, and pH 4.60 is reached after $t_{\mathrm{end}} = 6.07\,\mathrm{h}$. Nothing in Sections 3.2–3.4 depends on the Gompertz form itself. The rheological laws only need a strictly decreasing C^1 trajectory near pH_g, so a mechanistic fermentation module (starter growth, lactic acid production, buffering by the milk), such as the one of a stirred-yoghurt line model, can be used instead of (4) without touching the rheology.

3.2 Pre-gel sol branch and matching at the critical gel point

Before percolation ($\mathrm{pH} > \mathrm{pH}_g$), and only where the torque is measurable, the milk is described by a fractional Maxwell model (FMM) consisting of two springpots in series, $(\mathbb{V}_1, \alpha_1)$ and $(\mathbb{V}_2, \alpha_2)$ with $0 \le \alpha_2 < \alpha_1 \le 1$ [2]:

$$G^*_{\mathrm{FMM}}(\omega, t) = \left[\frac{1}{\mathbb{V}_1(t)(i\omega)^{\alpha_1(t)}} + \frac{1}{\mathbb{V}_2(t)(i\omega)^{\alpha_2(t)}}\right]^{-1}. \tag{6}$$

Multiplying numerator and denominator by the complex conjugate of $1 + (\mathbb{V}_1/\mathbb{V}_2)(i\omega)^{\alpha_1-\alpha_2}$ separates the storage and loss components explicitly:

$$G'_{\mathrm{FMM}}(\omega) = \frac{\mathbb{V}_1\omega^{\alpha_1}\cos\!\left(\frac{\pi\alpha_1}{2}\right) + \frac{\mathbb{V}_1^2}{\mathbb{V}_2}\omega^{2\alpha_1-\alpha_2}\cos\!\left(\frac{\pi\alpha_2}{2}\right)}{1 + 2\frac{\mathbb{V}_1}{\mathbb{V}_2}\omega^{\alpha_1-\alpha_2}\cos\!\left(\frac{\pi(\alpha_1-\alpha_2)}{2}\right) + \left(\frac{\mathbb{V}_1}{\mathbb{V}_2}\right)^2\omega^{2(\alpha_1-\alpha_2)}}, \tag{7}$$

$$G''_{\mathrm{FMM}}(\omega) = \frac{\mathbb{V}_1\omega^{\alpha_1}\sin\!\left(\frac{\pi\alpha_1}{2}\right) + \frac{\mathbb{V}_1^2}{\mathbb{V}_2}\omega^{2\alpha_1-\alpha_2}\sin\!\left(\frac{\pi\alpha_2}{2}\right)}{1 + 2\frac{\mathbb{V}_1}{\mathbb{V}_2}\omega^{\alpha_1-\alpha_2}\cos\!\left(\frac{\pi(\alpha_1-\alpha_2)}{2}\right) + \left(\frac{\mathbb{V}_1}{\mathbb{V}_2}\right)^2\omega^{2(\alpha_1-\alpha_2)}}. \tag{8}$$

When the terminal relaxation time diverges as percolation is approached ($\mathbb{V}_1 \to +\infty$ with $\mathbb{V}_2$ finite and $\alpha_2 \to n$), the two expressions tend to $\mathbb{V}_2\omega^n\cos(\pi n/2)$ and $\mathbb{V}_2\omega^n\sin(\pi n/2)$, so the sol branch joins the Winter–Chambon gel without a jump. We stop there. No pH laws are proposed for $(\mathbb{V}_1, \alpha_1, \mathbb{V}_2, \alpha_2)$; this branch only serves to approach the critical gel continuously, and the model becomes predictive at t_g.

3.3 Post-gel constitutive laws: dimensional homogeneity, Option A and Option B

A naive choice would be an exponential law written directly on $\ln(\mathbb{V}_\infty/\mathbb{V}_g)$. It is not dimensionally consistent once $\alpha(\mathrm{pH})$ varies: $[\mathbb{V}_g] = \mathrm{Pa\,s}^n$ while $[\mathbb{V}_\infty] = \mathrm{Pa\,s}^{\alpha_\infty}$, so the ratio has units of $\mathrm{s}^{\alpha_\infty - n}$. The fitted values would then depend on whether time is counted in seconds or in minutes, and α and $\mathbb{V}$ would become artificially correlated.

We avoid this by fixing a reference angular frequency $\omega_0 > 0$ (period $\tau_0 = \omega_0^{-1}$) and writing

$$\mathbb{V}(t) = G_0(t)\,\omega_0^{-\alpha(t)} = G_0(t)\,\tau_0^{\alpha(t)}, \qquad [G_0] = \mathrm{Pa}. \tag{9}$$

In the quasi-static oscillatory regime, (3) becomes strictly dimensionless in frequency:

$$G'(\omega,t) = G_0(t)\left(\frac{\omega}{\omega_0}\right)^{\alpha(t)}\cos\!\left(\frac{\pi\alpha(t)}{2}\right), \qquad G''(\omega,t) = G_0(t)\left(\frac{\omega}{\omega_0}\right)^{\alpha(t)}\sin\!\left(\frac{\pi\alpha(t)}{2}\right). \tag{10}$$

With $\omega_0 = \omega_{\mathrm{geom}} := \left(\prod_{j=1}^{M}\omega_j\right)^{1/M}$, $G_0(t) = |G^*(\omega_0, t)|$ is simply the magnitude of the complex modulus at the logarithmic centre of the measured band.

Option A (static pH parameterisation). Define the post-gel acidification progress $\Delta\mathrm{pH}(t) = \max(0, \mathrm{pH}_g - \mathrm{pH}(t)) \geq 0$. Option A sets

$$\alpha_{\mathrm{eq}}(\mathrm{pH}) = \alpha_\infty + (n - \alpha_\infty)\exp\!\left(-\frac{\Delta\mathrm{pH}}{w_\alpha}\right), \tag{11}$$

$$\ln\!\left(\frac{G_0(\mathrm{pH})}{G_g}\right) = \ln\!\left(\frac{G_\infty}{G_g}\right)\left[1 - \exp\!\left(-\frac{\Delta\mathrm{pH}}{w_G}\right)\right], \tag{12}$$

subject to $0 < \alpha_\infty < n < 1$, $0 < G_g < G_\infty$, $w_\alpha > 0$, and $w_G > 0$. At $\mathrm{pH} = \mathrm{pH}_g$, (11)–(12) reduce to $\alpha = n$ and $G_0 = G_g$; as acidification progresses, α decreases monotonically toward α_∞ while G_0 increases toward G_∞. We chose exponentials because they are the simplest functions with the right end values; logistic or power-law forms in $\Delta\mathrm{pH}$ deserve a comparison once laboratory spectra exist.

Option B (fractional structural lag). The network may not follow the bulk serum pH instantly [18]. In that case the exponent should relax towards $\alpha_{\mathrm{eq}}(\mathrm{pH}(t))$ rather than sit on it. Giusti

et al. used a relaxation equation with a constant target for the order function [11]; in Option B the constant is replaced by $\alpha_{\mathrm{eq}}(\mathrm{pH}(t))$ from (11):

$$ {}^{C}D^{\beta}_{t_g}\alpha(t) = -c\Big[\alpha(t) - \alpha_{\mathrm{eq}}(\mathrm{pH}(t))\Big], \qquad \alpha(t_g) = n, \qquad \beta \in (0,1], \quad c > 0. \tag{13} $$

The constant c has units $\mathrm{s}^{-\beta}$ and defines a structural relaxation time $\tau_{\mathrm{struct}} = c^{-1/\beta}$. For $\beta = 1$ the relaxation is exponential, and in the limit $c \to +\infty$ Option A is recovered.

Theorem 1 (Existence, uniqueness and interval invariance for Option B)**.** *Let* $\mathrm{pH} \in C([t_g, T])$ *satisfy* $\mathrm{pH}(t) \le \mathrm{pH}_g$ *on* $[t_g, T]$*, and let* α_{eq} *be defined by* (11) *with* $0 < \alpha_\infty < n < 1$*. For all* $\beta \in (0,1]$ *and* $c > 0$*, problem* (13) *possesses a unique continuous solution on* $[t_g, T]$*, given by*

$$ \alpha(t) = n\,E_\beta\big(-c(t-t_g)^\beta\big) + c\int_{t_g}^{t} (t-s)^{\beta-1}\,E_{\beta,\beta}\big(-c(t-s)^\beta\big)\,\alpha_{\mathrm{eq}}(\mathrm{pH}(s))\,ds, \tag{14} $$

where $E_\beta(z) = \sum_{k=0}^{\infty} z^k/\Gamma(\beta k + 1)$ *and* $E_{\beta,\beta}(z) = \sum_{k=0}^{\infty} z^k/\Gamma(\beta k + \beta)$ *denote the one- and two-parameter Mittag–Leffler functions. Moreover,*

$$ \alpha_\infty \le \alpha(t) \le n \qquad \forall t \in [t_g, T]. \tag{15} $$

If $t \mapsto \mathrm{pH}(t)$ *is non-increasing on* $[t_g, T]$*, then* $\alpha(t) \ge \alpha_{\mathrm{eq}}(\mathrm{pH}(t))$ *for all* $t \in [t_g, T]$*.*

Proof. Because (13) is linear with constant coefficient $-c$ and continuous forcing $c\,\alpha_{\mathrm{eq}}(\mathrm{pH}(t))$, extending $\alpha_{\mathrm{eq}}(\mathrm{pH}(t))$ continuously and boundedly to $[t_g, +\infty)$ (e.g., as a constant for $t > T$) allows Laplace inversion for Caputo equations of order $\beta \in (0,1]$, yielding existence, uniqueness in $C([t_g, T])$ and the variation-of-constants formula (14). By Pollard's theorem [22], $x \mapsto E_\beta(-x)$ is completely monotone on $[0, +\infty)$ for $\beta \in (0,1]$. In particular, $E_\beta(-c(t-t_g)^\beta) > 0$, and the resolvent kernel satisfies

$$ K_\beta(x) := c\,x^{\beta-1}E_{\beta,\beta}(-cx^\beta) = -\frac{d}{dx}\Big[E_\beta(-cx^\beta)\Big] \ge 0 \qquad \forall x > 0. $$

Integrating $K_\beta(t-s)$ over $s \in [t_g, t]$ yields the exact partition of unity

$$ E_\beta\big(-c(t-t_g)^\beta\big) + \int_{t_g}^{t} K_\beta(t-s)\,ds = E_\beta\big(-c(t-t_g)^\beta\big) + \Big[1 - E_\beta\big(-c(t-t_g)^\beta\big)\Big] = 1. $$

Equation (14) therefore represents $\alpha(t)$ as a convex combination of n and $\{\alpha_{\mathrm{eq}}(\mathrm{pH}(s))\}_{s\in[t_g,t]}$. Since $\alpha_\infty \le \alpha_{\mathrm{eq}}(\mathrm{pH}(s)) \le n$ throughout $[t_g, t]$, (15) follows immediately. If pH is non-increasing, then $\alpha_{\mathrm{eq}}(\mathrm{pH}(s)) \ge \alpha_{\mathrm{eq}}(\mathrm{pH}(t))$ for all $s \le t$ and $n \ge \alpha_{\mathrm{eq}}(\mathrm{pH}(t))$; positivity of the weights then gives $\alpha(t) \ge \alpha_{\mathrm{eq}}(\mathrm{pH}(t))$. □

3.4 Mutation number and variable-order creep formulations

The frequency-domain formulas (10) hold only while $\alpha(t)$ and $G_0(t)$ vary negligibly over the interrogation window Δt. Following Mours and Winter [7], we track the dimensionless mutation number

$$ N_{\mathrm{mu}}(t;\Delta t) = \frac{\Delta t}{g(t)}\left|\frac{\partial g(t)}{\partial t}\right| = \frac{\Delta t}{\tau_{\mathrm{mu}}(t)}. \tag{16} $$

Taking $g(t) = G'(\omega, t)$ under Option A produces the closed-form expression

$$ N_{\mathrm{mu}}(\omega, t;\Delta t) = \Delta t\left|\left[\frac{d\ln G_0}{d\mathrm{pH}} + \left(\ln\frac{\omega}{\omega_0} - \frac{\pi}{2}\tan\frac{\pi\alpha}{2}\right)\frac{d\alpha}{d\mathrm{pH}}\right]\frac{d\mathrm{pH}}{dt}\right|. \tag{17} $$

The most demanding moment for the quasi-static assumption comes right after the gel point: α is then at its largest, and $|d\ln G_0/d\mathrm{pH}|$ and $|d\alpha/d\mathrm{pH}|$ are both at their maximum.

Once N_{mu} reaches values of order 10^{-1}, the material can no longer be treated as frozen during a measurement, and a variable-order law has to be written in the time domain. We consider a step stress $\sigma(t) = \sigma_0 H(t - t_w)$ applied at a waiting time $t_w \geq t_g$ (with $\gamma(t) = 0$ for $t \leq t_w$) and compare three non-autonomous laws:

- **VO-I (naive Type I):** $\sigma(t) = \mathbb{V}(t)\, {}^{C}D_{t_w}^{\alpha(t),\mathrm{I}}\gamma(t)$, placing $\mathbb{V}(t) = G_0(t)\tau_0^{\alpha(t)}$ outside the integral.
- **VO-II (naive Type II):** $\sigma(t) = \mathbb{V}(t)\, {}^{C}D_{t_w}^{\alpha(\cdot),\mathrm{II}}\gamma(t)$.
- **VO-Inc (incremental hereditary law):**

$$\sigma(t) = \int_{t_w}^{t} \frac{\mathbb{V}(s)}{\Gamma(1-\alpha(s))}\,(t-s)^{-\alpha(s)}\,\dot{\gamma}(s)\,ds. \tag{18}$$

Why should the choice matter? In a gel that is still forming, a bond created at time s joins a network that is already strained, and it carries no stress at the moment it forms. Its stiffness $\mathbb{V}(s)$ should therefore multiply only the strain increments $\dot{\gamma}(s)\,ds$ that come after its creation, which is what (18) does. Putting $\mathbb{V}(t)$ in front of the integral amounts to asking late bonds to carry the whole earlier strain history, and the compliance can then decrease under a constant positive stress (Section 6.3). The idea itself is not new. In the solidification theory of concrete, aging is described as the growth of a load-bearing constituent that does not itself age [24]; Eq. (18) is essentially the fractional counterpart of that picture.

Remark (Thermodynamic consistency as an open problem). We do not know of a general proof of Clausius–Duhem admissibility for variable-order fractional laws, and we do not give one here. A fermenting milk gel is an open, chemically reacting system. Its free energy $\psi(\mathcal{H}_\gamma, \xi)$ depends on a progress variable $\xi(t)$ tied to lactic acid production and casein protonation, and the isothermal inequality reads $\sigma\dot{\gamma} - \rho\dot{\psi} = \mathcal{D}_{\mathrm{mech}} + \mathcal{A}\dot{\xi} \geq 0$, with chemical affinity $\mathcal{A} = -\rho\partial\psi/\partial\xi$. Showing that $\mathcal{D}_{\mathrm{mech}} \geq 0$ for (18) when $\alpha(s)$ decreases and $\mathbb{V}(s)$ increases would require an explicit internal-variable free energy, which we leave for later work.

3.5 Parameter inventory

In total, Option A has 11 parameters (4 for the acidification, 7 for the post-gel rheology), and Option B two more (β and c). Their units, bounds and the data from which each one is identified are listed in Table 1.

4 Numerical methods, identifiability and inference

4.1 Fisher information orthogonalisation in the frequency domain

For each OWCh spectrum acquired at time $t_k \geq t_g$ over M frequencies $\{\omega_j\}_{j=1}^{M}$, window-by-window fitting minimises the sum of squared residuals on log-moduli (corresponding to independent multiplicative log-normal noise of variance σ_ε^2):

$$y_{1,j} = \ln G'(\omega_j) = \ln G_0 + \alpha \ln\!\left(\frac{\omega_j}{\omega_0}\right) + \ln\cos\!\left(\frac{\pi\alpha}{2}\right) + \varepsilon_{1,j}, \tag{19}$$

$$y_{2,j} = \ln G''(\omega_j) = \ln G_0 + \alpha \ln\!\left(\frac{\omega_j}{\omega_0}\right) + \ln\sin\!\left(\frac{\pi\alpha}{2}\right) + \varepsilon_{2,j}. \tag{20}$$

No Mittag–Leffler evaluation is needed at this stage.

Table 1: Model parameters, physical dimensions, admissibility constraints and primary identification observables.

Parameter	Units	Admissible domain	Physical meaning	Identified from
pH_0, A	pH	$\mathrm{pH}_0 > A > 0$	Initial pH and total drop	pH(t) curve
μ_m	$\mathrm{pH\,h^{-1}}$	$\mu_m > 0$	Maximum acidification rate	pH(t) curve
λ	h	$\lambda \geq 0$	Fermentation lag time	pH(t) curve
pH_g	pH	$(\mathrm{pH}_0 - A, \mathrm{pH}(0))$	Gelation pH (≈ 4.9 unheated; higher if heated; T-dependent)	Multi-ω $\tan\delta$ crossing
n	–	$n \in (\alpha_\infty, 1)$	Critical gel exponent	Spectrum at $t = t_g$
α_∞, w_α	– ; pH	$\alpha_\infty \in (0, n)$; $w_\alpha > 0$	Terminal exponent and pH scale	Post-gel spectra
G_g, G_∞, w_G	Pa ; Pa ; pH	$0 < G_g < G_\infty$; $w_G > 0$	Reference moduli at ω_0 and pH scale	Post-gel spectra
β, c (Opt. B)	– ; $\mathrm{s}^{-\beta}$	$\beta \in (0, 1]$; $c > 0$	Lag order and relaxation rate	Multi-rate post-gel spectra

Proposition 2 (Exact local decorrelation of $\ln G_0$ and α)**.** *Let* $\theta_{\mathrm{loc}} = (\ln G_0, \alpha)^\top$ *and* $\omega_{\mathrm{geom}} = \exp(\frac{1}{M}\sum_{j=1}^{M} \ln \omega_j)$*. Under independent Gaussian errors of variance* σ_ε^2 *in* (19)–(20)*, the off-diagonal entry of the Fisher information matrix* $\mathcal{I}(\theta_{\mathrm{loc}}) = \sigma_\varepsilon^{-2} J^\top J$ *is*

$$\mathcal{I}_{12}(\theta_{\mathrm{loc}}) = \frac{2M}{\sigma_\varepsilon^2}\left[\ln\left(\frac{\omega_{\mathrm{geom}}}{\omega_0}\right) + \frac{\pi}{2}\cot(\pi\alpha)\right]. \tag{21}$$

Consequently: (i) when regressing on $|G^*(\omega_j)|$ *alone,* $\omega_0 = \omega_{\mathrm{geom}}$ *orthogonalises* $\ln G_0$ *and* α *exactly for all* $\alpha \in (0, 1)$*; (ii) in joint regression on* $(\ln G', \ln G'')$*, local correlation vanishes if and only if* $\omega_0 = \omega_0^*(\alpha) := \omega_{\mathrm{geom}} \exp(\frac{\pi}{2}\cot(\pi\alpha))$*, and geometric centring* $\omega_0 = \omega_{\mathrm{geom}}$ *achieves exact orthogonality at* $\alpha = 1/2$*.*

Proof. The rows of the Jacobian $J \in \mathbb{R}^{2M\times 2}$ are $\big(1,\, \ln(\omega_j/\omega_0) - \frac{\pi}{2}\tan(\frac{\pi\alpha}{2})\big)$ for $\ln G'$ and $\big(1,\, \ln(\omega_j/\omega_0) + \frac{\pi}{2}\cot(\frac{\pi\alpha}{2})\big)$ for $\ln G''$. Taking the inner product of the two columns gives

$$(J^\top J)_{12} = \sum_{j=1}^{M}\left[2\ln\frac{\omega_j}{\omega_0} + \frac{\pi}{2}\left(\cot\frac{\pi\alpha}{2} - \tan\frac{\pi\alpha}{2}\right)\right].$$

Using $\cot x - \tan x = 2\cot(2x)$ at $x = \pi\alpha/2$ simplifies the trigonometric term to $\pi\cot(\pi\alpha)$, yielding (21). Setting $\mathcal{I}_{12} = 0$ gives $\omega_0^*(\alpha)$ immediately; dropping the phase terms leaves $\ln(\omega_{\mathrm{geom}}/\omega_0) = 0$ for $|G^*|$ alone. □

4.2 L1 discretisation and sum-of-exponentials memory compression

Both Option B (13) and the Volterra creep laws are integrated on a uniform grid $t_k = t_0 + kh$ ($k = 0, \ldots, N$, $h = (T - t_0)/N$) using the L1 scheme. For constant order $\beta \in (0, 1)$,

$${}^{C}D_{t_0}^{\beta} y(t_k) \approx \frac{1}{\Gamma(2-\beta)\, h^\beta}\sum_{m=0}^{k-1} b_{k-1-m}\,(y_{m+1} - y_m), \qquad b_j = (j+1)^{1-\beta} - j^{1-\beta}. \tag{22}$$

For $y \in C^2([t_0, T])$ the scheme (22) is of order $O(h^{2-\beta})$. The solution of (13) is not smooth at the origin, though: with bounded forcing it behaves like $(t - t_0)^\beta$, so that $\dot{y}(t) \sim (t - t_0)^{\beta-1}$. On a uniform grid the L^∞ error then decays only like $O(h^\beta)$, even if the error at $t = T$ is still $O(h)$.

Graded meshes are the usual remedy [23]. A creep test has the same difficulty at its start, where $J \sim (t - t_w)^\alpha$, and this is why Section 6.3 uses a fine uniform mesh.

To invert the incremental creep law (18) for $\sigma(t_k) = 1$ ($J_k = J(t_k, t_w)$), piecewise-linear interpolation of J on $[t_m, t_{m+1}]$ with midpoint parameters $\bar{\alpha}_m = \frac{1}{2}(\alpha_m + \alpha_{m+1})$ and $\bar{G}_{0,m} = \sqrt{G_{0,m} G_{0,m+1}}$ ($\bar{\mathbb{V}}_m = \bar{G}_{0,m} \tau_0^{\bar{\alpha}_m}$) yields the lower-triangular marching scheme

$$J_k = J_{k-1} + \frac{1 - \sum_{m=0}^{k-2} W_{k,m} \, (J_{m+1} - J_m)}{W_{k,k-1}}, \tag{23}$$

with analytically integrated kernel weights

$$W_{k,m} = \frac{\bar{\mathbb{V}}_m}{\Gamma(2 - \bar{\alpha}_m) \, h} \Big[(t_k - t_m)^{1-\bar{\alpha}_m} - (t_k - t_{m+1})^{1-\bar{\alpha}_m} \Big], \qquad W_{k,k-1} = \frac{\bar{\mathbb{V}}_{k-1}}{\Gamma(2 - \bar{\alpha}_{k-1}) \, h^{\bar{\alpha}_{k-1}}}. \tag{24}$$

Evaluating the history directly costs $O(N^2)$ operations. A sliding window that forgets the distant past does not work with power-law memory (Section 6.2). A better route is to discretise the Laplace representation of the kernel,

$$t^{-\beta} = \frac{1}{\Gamma(\beta)} \int_0^\infty s^{\beta-1} e^{-st} \, ds = \frac{1}{\Gamma(\beta)} \int_{-\infty}^{+\infty} e^{\beta x - t e^x} \, dx \qquad (s = e^x), \tag{25}$$

with the trapezoidal rule on $[x_{\min}, x_{\max}]$, which gives a sum of $N_{\exp}$ exponentials (SOE) and a cost of $O(N \cdot N_{\exp})$. This applies directly to constant-order sums such as Option B. For variable-order kernels one would have to interpolate between SOE approximations built on a grid of fixed exponents.

4.3 Global estimation, model selection and software stack

For real data we plan two estimation routes. The first is sequential: acidification parameters from $\mathrm{pH}(t)$, then pH_g from the multi-frequency $\tan\delta$, then the post-gel parameters. The second is a joint Bayesian fit by MCMC with weakly informative priors. The prior on pH_g is $\mathcal{N}(4.9, 0.15^2)$ for unheated milk and $\mathcal{N}(5.3, 0.2^2)$ for heated milk, broad enough to include the values of Laligant et al. [18], and a separate pH_g is allowed at each temperature; the constraint $0 < \alpha_\infty < n < 1$ is imposed throughout. Three nested models are compared with the Akaike and Bayesian information criteria: constant order (M_0, $k = 5$ parameters, σ_ε^2 included), Option A (M_A, $k = 7$) and Option B (M_B, $k = 9$),

$$\mathrm{AIC} = N_{\mathrm{obs}} \ln\!\left(\frac{\mathrm{RSS}}{N_{\mathrm{obs}}}\right) + 2k, \qquad \mathrm{BIC} = N_{\mathrm{obs}} \ln\!\left(\frac{\mathrm{RSS}}{N_{\mathrm{obs}}}\right) + k \ln N_{\mathrm{obs}}, \tag{26}$$

and we also look at profile likelihoods and posterior correlations. As independent checks we intend to use `pyRheo` [19] for the springpot and FMM fits, and an inverse physics-informed neural network (PINN) for time-fractional rheology [20] as a second solver for Option B. Code and data will be archived with the final submission.

5 Proposed experimental protocol

A real test of the model needs $G'(\omega, t)$ and $G''(\omega, t)$ at several frequencies together with $\mathrm{pH}(t)$, all recorded on the same starter-fermented milk. Published curves (what we call Level 1) are often at a single frequency or obtained with GDL. Plant records (Level 3: tank pH and viscosity after stirring, but no $G'(t)$ in the tank) can only test the acidification module and the hand-over to a line model. The minimal laboratory campaign (Level 2) we have in mind is the following.

- **Factorial design ($3 \times 2 \times 2$):** three incubation temperatures (37, 40, 43°C), two starter inoculation levels (1% and 3%) and two milk heat treatments (unheated vs 80°C for 30 min), matching ranges in [16, 17]. The gelation pH is fitted separately for each temperature [18].
- **Replication and controls:** 12 starter-fermented conditions in duplicate (24 runs), plus one GDL control gel per heat treatment to isolate structural differences between chemical and microbial acidification.
- **Metrology:** linear-regime OWCh or multi-wave spectra ($\Delta t \in [5, 10]$ s, at least two decades such as $\omega \in [0.5, 50]\,\mathrm{rad\,s^{-1}}$) logged concurrently with a calibrated pH probe in a temperature-matched parallel vessel down to pH = 4.6.
- **Acceptance criteria:** RMSE on $\ln G'$ and $\ln G''$, discrepancy $|t_{g,\mathrm{pred}} - t_{g,\mathrm{meas}}|$ against Winter–Chambon crossover, and leave-one-condition-out prediction (e.g., predicting 40°C solely from parameters fitted at 37 and 43°C).

6 Analytical and numerical checks

Everything in this section was obtained analytically or with double-precision Python simulations. The aim is to check that the model is internally consistent, that the schemes converge and that the parameters can be identified. None of the numbers below is a measurement on milk.

6.1 Forward coupled dynamics and Fisher-matrix conditioning

Figure 2 shows the forward model for a heated milk with $\mathrm{pH}_0 = 6.65$, $A = 2.15$, $\mathrm{pH}_g = 5.20$, $n = 0.65$, $\alpha_\infty = 0.18$, $w_\alpha = 0.22$, $G_g = 2.0\,\mathrm{Pa}$, $G_\infty = 350\,\mathrm{Pa}$, $w_G = 0.18$ and $\omega_0 = 5.0\,\mathrm{rad\,s^{-1}}$. These numbers are only meant to be plausible. The value of α_∞ comes from caseinate gels [4], and n was chosen close to the critical exponent measured on rennet gels [9]. In panel (a), three assumed acidification rates stand for incubation at 37, 40 and 43°C ($\mu_m = 0.45$, 0.70 and $1.15\,\mathrm{pH\,h^{-1}}$, with $\lambda = 2.0$, 1.5 and 1.1 h); the gelation thresholds of heated (5.20) and unheated (4.90) milk are also shown. Panel (b) gives G' and G'' after the gel point at $\omega = 1$, 5 and $50\,\mathrm{rad\,s^{-1}}$ for the reference run at 40°C ($\mu_m = 0.70\,\mathrm{pH\,h^{-1}}$). Because $n = 0.65$ is larger than 0.5, G'' exceeds G' at all three frequencies right after $t_g = 3.68$ h. The curves cross simultaneously when α reaches 0.50, at $t \approx 3.86$ h, and G' then gains more than two decades while α drops towards 0.18.

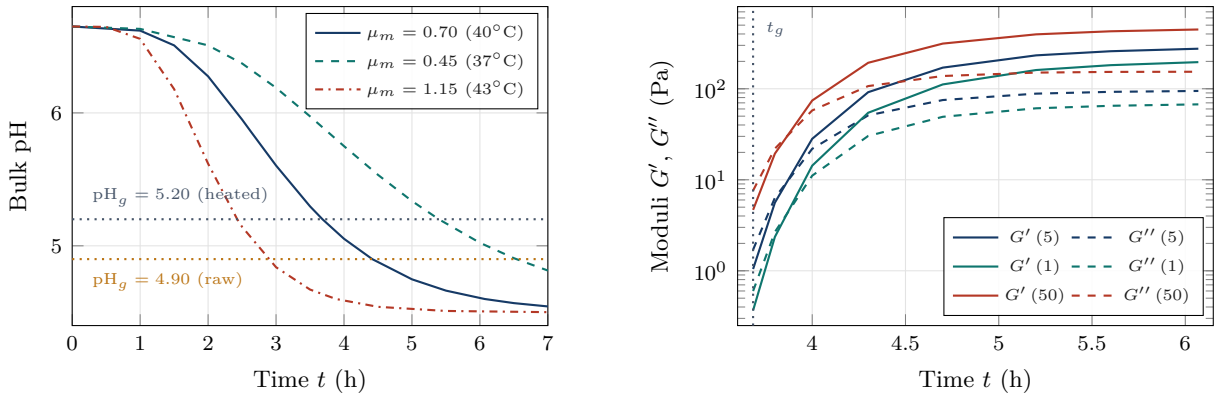

(a) Modified Gompertz acidification kinetics

(b) Post-gel G', G'' at $\omega \in \{1, 5, 50\}\,\mathrm{rad\,s^{-1}}$

Figure 2: Forward simulation with Option A. (a) Bulk pH for three acidification rates (μ_m in $\mathrm{pH\,h^{-1}}$). (b) Dynamic moduli after the gel point for the reference heated-milk run at 40°C ($\mathrm{pH}_g = 5.20$, $t_g = 3.68$ h).

To see what Proposition 2 means in practice, we computed the asymptotic correlation $\rho(\ln G_0, \alpha)$ and the condition number $\kappa(\mathcal{I})$ for a grid of 20 log-spaced frequencies between 0.5 and 50 $\mathrm{rad\,s^{-1}}$ ($\omega_{\mathrm{geom}} = 5.00\,\mathrm{rad\,s^{-1}}$). Three choices of ω_0 are compared in Table 2 and Figure 3: no centring ($\omega_0 = 1.0\,\mathrm{rad\,s^{-1}}$, which amounts to fitting $\ln \mathbb{V}$ in SI units), a fixed geometric centre ($\omega_0 = 5.0\,\mathrm{rad\,s^{-1}}$), and the α-dependent optimum $\omega_0^*(\alpha)$.

Table 2: Asymptotic correlation $\rho(\ln G_0, \alpha)$ and Fisher condition number $\kappa(\mathcal{I})$ on a 20-frequency OWCh grid ($[0.5, 50]\,\mathrm{rad\,s^{-1}}$, $\omega_{\mathrm{geom}} = 5.00\,\mathrm{rad\,s^{-1}}$).

α	Uncentred ($\omega_0 = 1$): ρ ; $\kappa(\mathcal{I})$	Geometric ($\omega_0 = 5$): ρ ; $\kappa(\mathcal{I})$	Exact $\omega_0^*(\alpha)$ ($\mathrm{rad\,s^{-1}}$) : ρ	$\lvert G^*\rvert$ only at ω_{geom}: ρ
0.65	−0.3384 ; 6.76	+0.3352 ; 6.73	2.25 : $< 10^{-15}$	0.00
0.50	−0.6078 ; 12.44	0.0000 ; 4.42	5.00 : $< 10^{-15}$	0.00
0.25	−0.7713 ; 45.03	−0.5136 ; 13.49	24.1 : $< 10^{-15}$	0.00
0.18	−0.7827 ; 73.55	−0.6062 ; 27.58	59.4 : $< 10^{-15}$	0.00

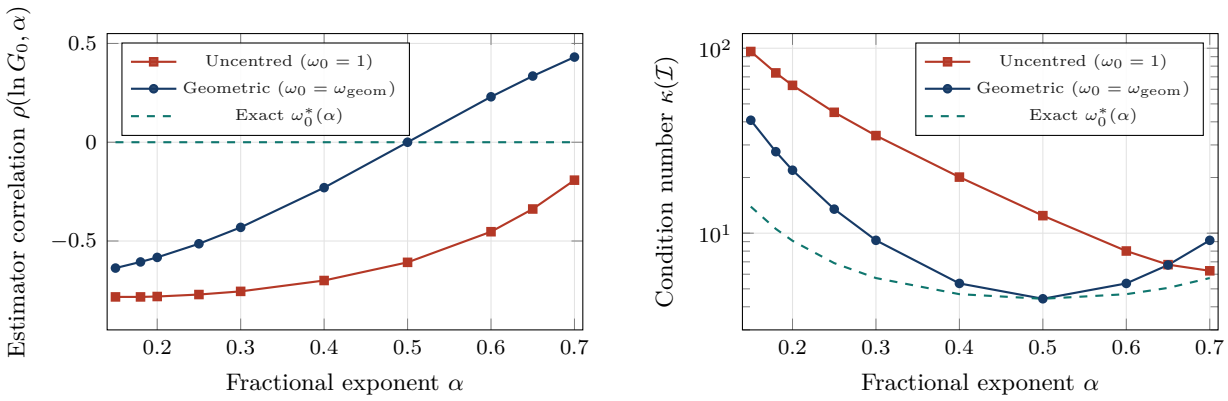

(a) Local parameter correlation

(b) Fisher matrix condition number

Figure 3: Effect of reference frequency ω_0 on local identifiability across the post-gel exponent range $\alpha \in [0.15, 0.70]$. Geometric centring lowers $\kappa(\mathcal{I})$ by a factor between 2.1 and 3.8 for $\alpha \leq 0.55$. What is left of the correlation comes from the phase term $\frac{\pi}{2}\cot(\pi\alpha)$.

With the optimal $\omega_0^*(\alpha)$ the correlation is zero to machine precision, as it should be. One detail of Figure 3(b) may look odd at first: for α above roughly 0.66, the uncentred fit is slightly better conditioned than the geometric one. The reason is that ω_0^* drops below ω_{geom} when $\cot(\pi\alpha) < 0$, and $1\,\mathrm{rad\,s^{-1}}$ then happens to be closer to it; at $\alpha = 0.65$ both choices give practically the same value ($\kappa = 6.76$ against 6.73). In the range that matters for a stiffening and mature gel, $\alpha \in [0.18, 0.55]$, the fixed geometric centre divides $\kappa(\mathcal{I})$ by 2.1 to 3.8.

6.2 Convergence of L1 solvers, SOE compression and mutation regimes

We checked the L1 schemes against three exact solutions (Figure 4(a)):

1. *Smooth Caputo derivative* ($y(t) = t^2$ on $[0, 1]$, $N \in \{40, 80, 160, 320, 640\}$): empirical orders converge to $2 - \beta$, measuring 1.495 for $\beta = 0.50$ (error 2.88×10^{-5} at $N = 640$) and 1.249 for $\beta = 0.75$ (error 2.20×10^{-4}).

2. *Option B with constant target* ($y(t) = \alpha_\infty + (n - \alpha_\infty)E_\beta(-ct^\beta)$, $c = 1.2$): because of the initial t^β singularity, global L^∞ convergence on a uniform mesh drops to $O(h^\beta)$ (0.474 → 0.50 at $\beta = 0.50$; 0.750 at $\beta = 0.75$), whereas endpoint error at $t = T$ maintains first-order scaling (1.010 and 1.026, reaching 4.93×10^{-5} and 9.05×10^{-5} at $N = 640$).

3. *Constant-order Volterra creep inversion* ($\alpha = 0.35$, $G_0 = 50\,\mathrm{Pa}$, $\tau_0 = 0.2\,\mathrm{s}$, $T = 100\,\mathrm{s}$, exact $J(100\,\mathrm{s}) = 0.197569\,\mathrm{Pa}^{-1}$): VO-I and VO-II agree to 2.81×10^{-16} and converge at order 1.002 (relative error 2.19×10^{-4} at $N = 800$).

Memory compression was tested on $[0.5, 600]\,\mathrm{s}$ with $N = 1200$ and $h = 0.5\,\mathrm{s}$. Simply truncating the history does not work: keeping half of it ($W = 600$ steps) still leaves a 61.1% error on the creep compliance, and 354% with $W = 50$. The trapezoidal SOE approximation (25) on $x \in [-20, 10]$ with $\beta = 0.5$, by contrast, keeps the relative kernel error below 9.25×10^{-4} with only $N_{\mathrm{exp}} = 30$ exponentials.

Table 3 and Figure 4(b) give the mutation number (17) for two cases: a slow starter fermentation ($\mu_m = 0.70\,\mathrm{pH\,h^{-1}}$, $\lambda = 1.50\,\mathrm{h}$, $t_{\mathrm{end}} = 6.07\,\mathrm{h}$) and a fast, GDL-like acidification ($\mu_m = 3.50\,\mathrm{pH\,h^{-1}}$, $\lambda = 0.20\,\mathrm{h}$, $t_{\mathrm{end}} = 1.11\,\mathrm{h}$).

Table 3: Minimum mutation time τ_{mu} and peak mutation number $\max N_{\mathrm{mu}}$ across post-gel acidification.

Acidification regime	Protocol (Δt)	$\min \tau_{\mathrm{mu}}$ (s) at $\omega = 1$	$\max N_{\mathrm{mu}}$ ($\omega = 1$)	$\max N_{\mathrm{mu}}$ ($\omega = 5$)	$\max N_{\mathrm{mu}}$ ($\omega = 50$)
Slow ($0.70\,\mathrm{pH\,h^{-1}}$)	OWCh (5 s)	189.4	0.0264	0.0240	0.0205
Slow ($0.70\,\mathrm{pH\,h^{-1}}$)	OWCh (10 s)	189.4	0.0528	0.0480	0.0411
Slow ($0.70\,\mathrm{pH\,h^{-1}}$)	Sweep (180 s)	189.4	0.9505	0.8636	0.7393
Fast ($3.50\,\mathrm{pH\,h^{-1}}$)	OWCh (5 s)	37.9	0.1320	0.1199	0.1027
Fast ($3.50\,\mathrm{pH\,h^{-1}}$)	Sweep (180 s)	37.9	4.753	4.318	3.696

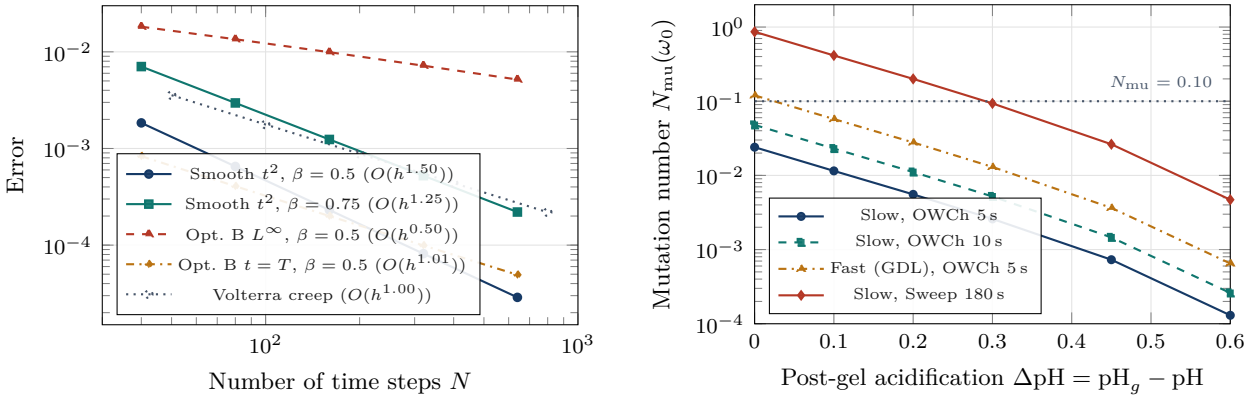

(a) Verified L1 convergence rates

(b) Mutation number along post-gel stiffening

Figure 4: (a) Convergence of the L1 Caputo and Volterra creep solvers, compared with exact solutions. (b) Mutation number at $\omega_0 = 5\,\mathrm{rad\,s^{-1}}$ as a function of the pH drop after gelation. During a lactic fermentation, 5 s chirps remain well inside the quasi-static range; a 180 s sequential frequency sweep leaves it near t_g.

In the slow case the shortest mutation time is 190 to 245 s, depending on frequency. This is of the same order as the 120 s or so expected for the GDL–caseinate gel of Geri et al. [6], but our own fast, GDL-like case gives 38 to 49 s, so the comparison says little beyond orders of magnitude. The practical message is clearer: a 5 s chirp keeps $N_{\mathrm{mu}} \leq 0.027$ during the whole fermentation, whereas a classical 180 s frequency sweep reaches $N_{\mathrm{mu}} \approx 0.95$ shortly after gelation.

6.3 Quasi-static versus variable-order creep and non-physical recoil

We then compared the three laws in creep. A unit stress is applied at $t_w = t_g + 60\,\mathrm{s}$, where the gel changes fastest ($\tau_{\mathrm{mu}}(\omega_0) = 222\,\mathrm{s}$, $\alpha(t_w) = 0.632$, $G_0(t_w) = 2.53\,\mathrm{Pa}$), and the response is followed for 600 s. Since J grows like $(\Delta t)^\alpha$ at short times, a coarse grid is not adequate here, and we used $N = 19\,200$ steps ($h = 0.031\,\mathrm{s}$). Halving the step changes J by less than 0.2% at $\Delta t = 5\,\mathrm{s}$ and by less than 0.03% after 60 s. With $h = 0.5\,\mathrm{s}$ we had first obtained a gap of 3.9% between the

quasi-static and incremental compliances at $\Delta t = 5\,\mathrm{s}$; the converged value is 1.1%. The results are given in Table 4 and Figure 5(a).

Table 4: Simulated creep compliance $J(\Delta t, t_w)$ (Pa^{-1}) initiated at $t_w = t_g + 60\,\mathrm{s}$ ($\tau_{\mathrm{mu}}(\omega_0) = 222.2\,\mathrm{s}$). Asterisks mark non-physical negative creep increments under constant positive stress.

Δt (s)	$N_{\mathrm{mu}}(\Delta t)$	J_{QS}	$J_{\mathrm{VO\text{-}I}}$	$J_{\mathrm{VO\text{-}II}}$	$J_{\mathrm{VO\text{-}Inc}}$	$\lvert J_{\mathrm{QS}} - J_{\mathrm{VO\text{-}Inc}}\rvert / J_{\mathrm{VO\text{-}Inc}}$
5	0.023	3.3718	3.3163	3.3201	3.3361	1.07%
10	0.045	5.2269	5.0651	5.0791	5.1280	1.93%
30	0.135	10.4709	9.5084	9.6103	9.8882	5.89%
60	0.270	16.2316	13.3398	13.6744	14.4642	12.22%
120	0.540	25.1616	16.9879	18.0049	20.0640	25.41%
300	1.350	44.9162	17.7248*	21.3269	27.0102	66.29%
600	2.701	69.6273	13.4021*	20.7875*	29.9266	132.66%

Up to $N_{\mathrm{mu}} \approx 0.05$ the quasi-static compliance is within 2% of the incremental one, and the three variable-order laws differ by at most 1.3%. The quasi-static error grows quickly afterwards and reaches 12% at $N_{\mathrm{mu}} \approx 0.27$. More striking is the behaviour of the two naive laws, which end up predicting a decreasing strain under a constant positive stress: VO-I reaches its maximum at $\Delta t \approx 212\,\mathrm{s}$ ($N_{\mathrm{mu}} \approx 0.96$), VO-II at $\Delta t \approx 352\,\mathrm{s}$ ($N_{\mathrm{mu}} \approx 1.6$). The recoil comes from weighting past strain increments with the present, stiffer prefactor $\mathbb{V}(t)$. With VO-Inc (18), J increases at every step.

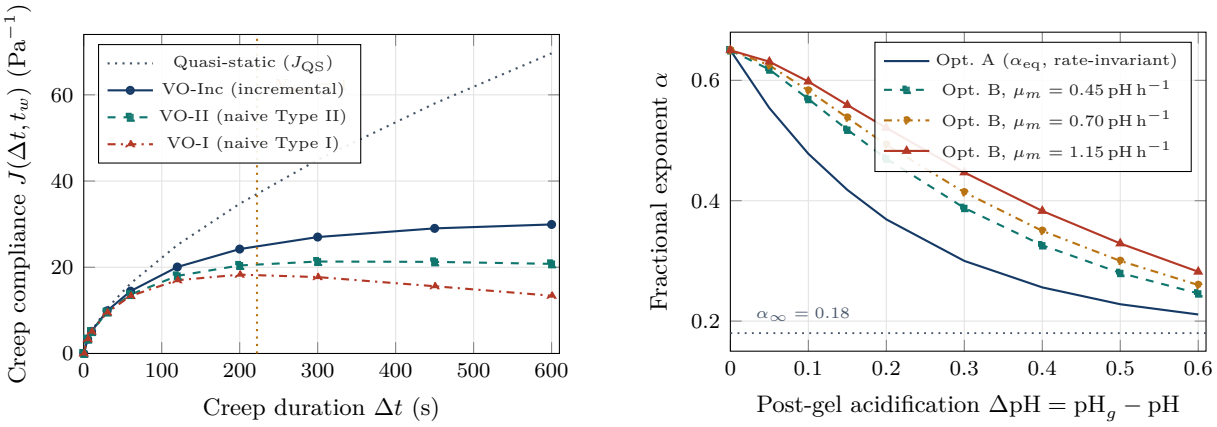

(a) Creep divergence and naive-law recoil

(b) Rate-dependent splitting under Option B

Figure 5: (a) Creep compliance for a stress applied at $t_w = t_g + 60\,\mathrm{s}$. VO-I and VO-II turn downward near $N_{\mathrm{mu}} \approx 1$ and 1.6; VO-Inc stays monotone. (b) Lag of the exponent in Option B ($\beta = 0.70$, $c = 0.008\,\mathrm{s}^{-0.7}$) compared with Option A. The lag $\alpha - \alpha_{\mathrm{eq}}$ grows with the acidification rate, and this is what makes the lag parameters identifiable when several rates are fitted together.

6.4 Model selection and multi-rate identifiability on synthetic data

For the model-selection test we generated synthetic OWCh spectra at 25 times after the gel point and 12 frequencies in $[0.5, 50]\,\mathrm{rad\,s^{-1}}$, that is $N_{\mathrm{obs}} = 600$ log-moduli per run, with 3% independent log-normal noise ($\sigma_\varepsilon = 0.03$). The data were produced either by Option A (Scenario 1) or by Option B with $\beta = 0.70$ and $c = 0.008\,\mathrm{s}^{-0.7}$ (Scenario 2), which gives a maximum lag $|\alpha_B - \alpha_A| = 0.1235$ at $\mu_m = 0.70\,\mathrm{pH\,h^{-1}}$. Single-run results are in Table 5.

In Scenario 1 the information criteria pick the right model. Option A beats the constant-order model by a wide margin ($\Delta\mathrm{BIC} = -2567$) and Option B by a smaller one ($\Delta\mathrm{BIC} = -12.8$), and all true values fall inside the 95% confidence intervals: $n = 0.6525 \pm 0.0046$ (true value 0.6500),

Table 5: Model comparison on synthetic single-condition OWCh spectra ($N_{\mathrm{obs}} = 600$, $\sigma_\varepsilon = 3\%$). Bold entries denote the lowest AIC and BIC.

Ground truth	Fitted model	$\mathrm{RMSE}_{\ln G'}$	$\mathrm{RMSE}_{\ln G''}$	AIC	BIC
Scenario 1 (Opt. A)	M_0 (const. α)	0.2637	0.2626	−1591.9	−1569.9
Scenario 1 (Opt. A)	M_A (Option A)	0.0297	0.0316	**−4168.1**	**−4137.3**
Scenario 1 (Opt. A)	M_B (Option B)	0.0297	0.0316	−4164.1	−4124.5
Scenario 2 (Opt. B)	M_0 (const. α)	0.2595	0.2641	−1598.3	−1576.3
Scenario 2 (Opt. B)	M_A (Option A)	0.0351	0.0350	−4005.8	−3975.0
Scenario 2 (Opt. B)	M_B (Option B)	0.0304	0.0323	**−4136.5**	**−4097.0**

$\alpha_\infty = 0.1814 \pm 0.0033$ (0.1800), $w_\alpha = 0.2169 \pm 0.0056$ (0.2200), $\ln G_g = 0.6945 \pm 0.0114$ (0.6931), $\ln G_\infty = 5.8574 \pm 0.0074$ (5.8579) and $w_G = 0.1796 \pm 0.0010$ (0.1800).

Scenario 2 is more instructive for the design of experiments. Given a single fermentation, BIC does select Option B ($\Delta\mathrm{BIC} = -122.0$ against Option A), but the equilibrium and lag parameters cannot be separated: $w_\alpha = 0.113 \pm 0.293$, $\beta = 0.802 \pm 0.530$, $\log_{10} c = -2.69 \pm 2.33$. Figure 5(b) suggests the way out. The lag $\alpha - \alpha_{\mathrm{eq}}$ depends on how fast the pH falls, while $\alpha_{\mathrm{eq}}(\Delta\mathrm{pH})$ does not, so runs at different rates carry complementary information. Fitting three rates at once ($\mu_m \in \{0.45, 0.70, 1.15\}\,\mathrm{pH\,h^{-1}}$, standing for 37, 40 and 43°C; $N_{\mathrm{obs}} = 1800$) is enough:

- $w_\alpha = 0.2164 \pm 0.0079$ (true 0.2200; uncertainty reduced 37-fold),
- $\beta = 0.6965 \pm 0.0259$ (true 0.7000; uncertainty reduced 20-fold),
- $\log_{10} c = -2.0922 \pm 0.0817$ (true −2.0969; uncertainty reduced 28-fold).

We also left the 40°C run out, fitted the two others ($\mu_m = 0.45$ and $1.15\,\mathrm{pH\,h^{-1}}$) and predicted it. Option B then reaches the 3% noise level ($\mathrm{RMSE}_{\ln G'} = 0.0306$, $\mathrm{RMSE}_{\ln G''} = 0.0334$), against 0.0332 and 0.0366 for Option A.

7 Discussion

Two of the parameters have a direct meaning for the product. The terminal exponent α_∞ tells how wide the relaxation spectrum of the set gel is, and G_∞ is its stiffness at ω_0 before any shearing. We insist on starter-fermented milk, rather than GDL gels, for two reasons: the textures can differ [15], and the transfer of acid and protons to the colloidal phase is not the same in the two cases [18]. Option B is a crude way of accounting for proton-transfer and rearrangement delays, with two parameters instead of a reaction–diffusion model.

The present work has clear limits.

1. *No new experimental data.* Section 6 shows that the model is consistent, that the schemes are accurate and that the parameters are identifiable. It says nothing about whether the exponential maps (11)–(12) actually describe fermented milk.
2. *Linear viscoelasticity only.* Large-strain yielding, breakdown during pumping and smoothing, and syneresis are outside the scope of (10) and (18).
3. *Temperature.* In the multi-rate test of Section 6.4, pH_g, w_α, G_g, G_∞ and c are the same at 37 and 43°C. For pH_g this is certainly wrong: Laligant et al. found it about 0.3 unit higher at 42°C than at 30°C. The same authors report equal G' at pH 4.6 at both temperatures, which makes a constant G_∞ acceptable as a first guess [18]. In the laboratory campaign

pH_g will be fitted at each temperature, and temperature-dependent forms, for instance an Arrhenius law for $c(T)$, will be tested.

8 Conclusion

The model proposed here connects lactic acidification to the linear viscoelastic spectra of yoghurt, from the gel point to the set gel. Writing $\mathbb{V}(t) = G_0(t)\,\omega_0^{-\alpha(t)}$ makes the parameters independent of the time unit and the fit better conditioned. In the lag model (Option B), Pollard's theorem keeps α between its terminal and critical values. The creep simulations justify a quasi-static reading of 5 s chirps ($N_{\mathrm{mu}} < 0.03$); they also show that the prefactor has to be placed inside the hereditary integral, as in (18), if a spurious recoil near $N_{\mathrm{mu}} \approx 1$ is to be avoided.

At pH 4.6 the model delivers a pair $(\alpha(t_{\mathrm{end}}),\, G_0(t_{\mathrm{end}}))$ that a stirred-yoghurt line model can take as its initial state. The viscosity after pumping, cooling and smoothing could then be related to the stiffness and to the loss tangent $\tan(\pi\alpha_{\mathrm{end}}/2)$ of the curd, and not only to the final pH. What remains is to calibrate the model on published curves and then to carry out the campaign of Section 5.

Data and code availability

No experimental data were generated in this work. The simulation scripts that reproduce the analytical checks, tables and figures will be deposited with the public version of this preprint.

References

[1] Faber, T.J., Jaishankar, A., McKinley, G.H., Describing the firmness, springiness and rubberiness of food gels using fractional calculus. Part I: Theoretical framework, *Food Hydrocolloids* 62, 311–324 (2017).

[2] Wagner, C.E., Barbati, A.C., Engmann, J., Burbidge, A.S., McKinley, G.H., Quantifying the consistency and rheology of liquid foods using fractional calculus, *Food Hydrocolloids* 69, 242–254 (2017).

[3] Bonfanti, A., Kaplan, J.L., Charras, G., Kabla, A., Fractional viscoelastic models for power-law materials, *Soft Matter* 16, 6002–6020 (2020).

[4] Keshavarz, B., Divoux, T., Manneville, S., McKinley, G.H., Nonlinear viscoelasticity and generalized failure criterion for polymer gels, *ACS Macro Letters* 6, 663–667 (2017). doi:10.1021/acsmacrolett.7b00213

[5] Divoux, T., Keshavarz, B., Leocmach, M., Quasi-properties and fractional constitutive equations for protein gels: connecting gel microstructure to power-law linear rheology, abstract, 88th Annual Meeting of the Society of Rheology, Tampa, FL (2017).

[6] Geri, M., Keshavarz, B., Divoux, T., Clasen, C., Curtis, D.J., McKinley, G.H., Time-resolved mechanical spectroscopy of soft materials via optimally windowed chirps, *Physical Review X* 8, 041042 (2018).

[7] Mours, M., Winter, H.H., Time-resolved rheometry, *Rheologica Acta* 33, 385–397 (1994). doi:10.1007/BF00366581

[8] Perego, A., Vadillo, D.C., Mills, M.J.L., et al., Evaluation of optimally windowed chirp signals in industrial rheological measurements: method development and data processing, *Rheologica Acta* 64, 391 (2025).

[9] Bauland, J., Manna, G., Divoux, T., Gibaud, T., Two-step aging dynamics in enzymatic milk gels, *Physical Review Materials* (2024); arXiv:2403.10176.

[10] Joshi, Y.M., Analysing gelation transition through fractional viscoelasticity and Mittag-Leffler-Prabhakar function, arXiv:2606.26656 (2026).

[11] Giusti, A., Colombaro, I., Garra, R., Garrappa, R., Mentrelli, A., On variable-order fractional linear viscoelasticity, *Fractional Calculus and Applied Analysis* 27, 1564–1578 (2024). doi:10.1007/s13540-024-00288-y

[12] Garrappa, R., Giusti, A., Mainardi, F., Variable-order fractional calculus: a change of perspective, *Communications in Nonlinear Science and Numerical Simulation* 102, 105904 (2021).

[13] Di Paola, M., Alotta, G., Burlon, A., Failla, G., A novel approach to nonlinear variable-order fractional viscoelasticity, *Philosophical Transactions of the Royal Society A* (2020). doi:10.1098/rsta.2019.0296

[14] Phadungath, C., The mechanism and properties of acid-coagulated milk gels, *Songklanakarin Journal of Science and Technology* 27, 433–448 (2005).

[15] Özcan, T., Horne, D.S., Lucey, J.A., Yogurt made from milk heated at different pH values, *Journal of Dairy Science* 98, 6749–6758 (2015).

[16] Soukoulis, C., Panagiotidis, P., Koureli, R., Tzia, C., Industrial yogurt manufacture: monitoring of fermentation process and improvement of final product quality, *Journal of Dairy Science* (2007).

[17] Alvarado, U., Tacuri, J., Coloma, A., Gallegos Rojas, E., Callo, H., Valencia-Sullca, C., Rafael, N.C., Castillo, M., Development of a hybrid system based on the CIELAB colour space and artificial neural networks for monitoring pH and acidity during yogurt fermentation, *Dairy* 6, 41 (2025). doi:10.3390/dairy6040041

[18] Laligant, A., Famelart, M.-H., Paquet, D., Brulé, G., Fermentation by lactic bacteria at two temperatures of pre-heated reconstituted milk. II – Dynamic approach of the gel construction, *Lait* 83, 307–320 (2003). doi:10.1051/lait:2003018

[19] Miranda-Valdez, I.Y., Niinistö, A., Mäkinen, T., Lejon, J., Koivisto, J., Alava, M.J., pyRheo: an open-source Python package for complex rheology, *Digital Discovery* 4, 1075 (2025). doi:10.1039/d5dd00021a

[20] Thakur, S., Mitra, H., Ardekani, A.M., Physics-informed neural network-based inverse framework for time-fractional differential equations for rheology, *Biology* 14, 779 (2025).

[21] Winter, H.H., Chambon, F., Analysis of linear viscoelasticity of a crosslinking polymer at the gel point, *Journal of Rheology* 30, 367–382 (1986). doi:10.1122/1.549853

[22] Pollard, H., The completely monotonic character of the Mittag-Leffler function $E_a(-x)$, *Bulletin of the American Mathematical Society* 54, 1115–1116 (1948).

[23] Stynes, M., O'Riordan, E., Gracia, J.L., Error analysis of a finite difference method on graded meshes for a time-fractional diffusion equation, *SIAM Journal on Numerical Analysis* 55, 1057–1079 (2017). doi:10.1137/16M1082329

[24] Bažant, Z.P., Prasannan, S., Solidification theory for concrete creep. I: Formulation, *Journal of Engineering Mechanics* 115, 1691–1703 (1989).